

RESEARCH ARTICLE | FEBRUARY 22 2024

## Cloud and droplet dynamics during a human coughing event under fully mixed and unmixed room conditions

Special Collection: [Flow and the Virus](#)

Arthur Hajaali   ; Thorsten Stoesser  ; Shaun Fitzgerald 

 Check for updates

*Physics of Fluids* 36, 023345 (2024)

<https://doi.org/10.1063/5.0185686>

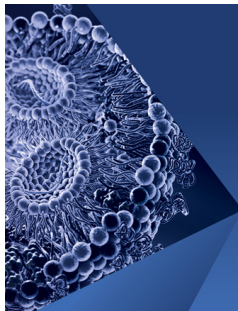


View  
Online



Export  
Citation

CrossMark



## Physics of Fluids

Special Topic:

Flow and Lipid Nanoparticles

Guest Editors: Richard Braatz and Mona Kanso

[Submit Today!](#)

# Cloud and droplet dynamics during a human coughing event under fully mixed and unmixed room conditions

Cite as: Phys. Fluids **36**, 023345 (2024); doi: [10.1063/5.0185686](https://doi.org/10.1063/5.0185686)

Submitted: 1 November 2023 · Accepted: 24 January 2024 ·

Published Online: 22 February 2024





View Online



Export Citation



CrossMark

Arthur Hajaali,<sup>1,a)</sup>  Thorsten Stoesser,<sup>1,b)</sup>  and Shaun Fitzgerald<sup>2,c)</sup> 

## AFFILIATIONS

<sup>1</sup>Department of Civil, Environmental and Geomatic Engineering, University College London, London WC1E 6BT, United Kingdom

<sup>2</sup>Centre for Climate Repair, Department of Engineering, University of Cambridge, Cambridge CB2 1PZ, United Kingdom

Note: This paper is part of the special topic, Flow and the Virus.

<sup>a)</sup> Author to whom correspondence should be addressed: [a.hajaali@ucl.ac.uk](mailto:a.hajaali@ucl.ac.uk)

<sup>b)</sup> Electronic mail: [t.stoesser@ucl.ac.uk](mailto:t.stoesser@ucl.ac.uk)

<sup>c)</sup> Electronic mail: [sdf10@cam.ac.uk](mailto:sdf10@cam.ac.uk)

## ABSTRACT

The study of cloud and droplet dynamics during potential transmission events, such as coughing, is essential for understanding the spread and deposition of aerosols and droplets carrying airborne diseases. This paper reports the refinement of a complex model that couples momentum, temperature, and humidity for accurately simulating the dynamics of aerosol clouds and the dispersion of larger droplets under various conditions within an environmental chamber. The model is then employed to quantify aerosol/droplet exposure of a person standing 1 m away from a host. In addition, a statistical framework sheds light on the impact of backward coupling (droplet to cloud), which is negligible compared to forward coupling (cloud to droplet). The near-field study also provides detailed information on droplet behavior, laying the foundation for large-scale far-field studies.

© 2024 Author(s). All article content, except where otherwise noted, is licensed under a Creative Commons Attribution (CC BY) license (<http://creativecommons.org/licenses/by/4.0/>). <https://doi.org/10.1063/5.0185686>

## I. INTRODUCTION

In late 2019, a novel coronavirus (CoV19) emerged in Wuhan, China, and rapidly spread around the world, causing the COVID pandemic. It has been suggested that the severe acute respiratory syndrome coronavirus 2 (SARS-CoV-2) is primarily transmitted through respiratory droplets produced when an infectious person talks, coughs, or sneezes.<sup>1–9</sup> Hence, a detailed understanding of the physics of the dispersion of respiratory droplets is crucial for developing effective interventions to mitigate the spread of the virus. During a coughing event, the exhaled breath is composed of aerosols and larger droplets. The threshold size differentiating an aerosol and a large droplet is the subject of an ongoing debate, but most of the community agrees that droplets under 10  $\mu\text{m}$  can be considered aerosols. Some of the smaller droplets can become aerosolized after partial evaporation. These aerosolized droplets can remain suspended for long periods and consequently can be carried with air currents. Environmental conditions, including temperature, humidity, and ambient airflow, altered by ventilation, significantly impact the behavior of the aerosol cloud and

individual droplets.<sup>10–15</sup> They affect not only the rate of droplet evaporation but also the external forces to which each droplet is subjected.

Numerical studies have helped increase our understanding of the dynamics of aerosols and droplets.<sup>16,17</sup> However, they rely on multi-factorial inputs that are challenging to capture and assess experimentally. These factors include the mass expelled, the time-dependent velocity profile, the number of particles, their distribution and time of release, the size of the mouth, and angles at which the cloud (or puff) is expelled, making it complex to simulate.<sup>18,19</sup> Numerous models have been developed to account for these parameters, attempting to account for the droplet's evaporation on their dynamics.<sup>20–24</sup> Some of these models use the Eulerian–Eulerian method to represent the infectious aerosol cloud with a scalar.<sup>25,26</sup> In contrast, others represent the cloud using an Eulerian–Lagrangian model in which the aerosols/droplets are tracked as individual particles.

Coughing under various conditions and types of spaces has been recently investigated to assess the risk of infection for a given individual based on their distance from an infected person.<sup>27</sup>

Dbouk and Drikakis<sup>28</sup> utilized fully coupled Eulerian–Lagrangian techniques to explore the transport and dispersion behavior of evaporating saliva particles from a human cough. This investigation considered various horizontal linear wind conditions, ranging from 1.1 to 4.2 m/s. This study differs in the calculation of the surface droplet temperature; instead of using the energy equation based on the enthalpy difference, our methodology captures the temperature and humidity from two scalar fields. The viral inhalation of a person standing at 1 m is approximately 10 times higher than for a person positioned at 2 m away from the infected individual under windy conditions (2 m/s). The evaporation time of the 50- $\mu\text{m}$  droplets triples when considering the salt mass fraction within the droplet.<sup>15</sup> The impact of fans and air ventilation was studied for a closed space including offices and elevators.<sup>29,30</sup> Although it revealed that the location of the ventilation system has a significant role in the dispersion of aerosol droplets, it will not eliminate the droplets. Partitioning of space was another method thought to reduce infection risk in the working space environment. On its own, it was judged not ineffective as it leads to local accumulation while reducing drastically the risk of infection when paired with an air purifier for each compartment.<sup>29</sup>

The study presented here involves the refinement of an existing model, coupling the Eulerian-based three-dimensional Navier–Stokes equations with three scalar transport equations, which enable one to determine the transport of aerosol–cloud concentration, temperature, and absolute humidity, respectively. The scalars are subsequently used to inform the evaporation model of individual large droplets, which, in turn, impact the size and dynamics of these discrete particles which are treated in a Lagrangian framework. The evaporated volume is coupled with the Eulerian framework, altering the temperature and humidity of the cell in which the particle(s) is/are located. The impact of the surrounding environment on the cloud and droplet dynamics is investigated.

In the first simulation, the mannequin coughs into a room where the surrounding velocity field is equal to zero, while in the second simulation, the mixing fan is turned on creating a well-mixed environment in which the mannequin’s coughing event occurs. The hydrodynamics and evaporation properties of the large Lagrangian droplets are individually monitored at every time step, enabling a detailed statistical analysis of the droplets. The exposure of a healthy person one meter away from the infected person was investigated under the two aforementioned room conditions.

## II. METHODOLOGY

### A. Numerical framework

#### 1. Continuous phase

The simulations utilize Hydro3D, an open-source Large Eddy Simulation (LES) code available at <https://github.com/Hydro3DTeam/hydro3D>. This code discretizes the governing filtered Navier–Stokes equations [Eq. (1)] through a finite-difference method on a Cartesian staggered grid. The filtering process is solely based on the fluid cell’s volume, represented as  $\Delta = (\Delta x \Delta y \Delta z)^{1/3}$ . Motion scales larger than the filter cutoff are resolved by discretizing the partial differential equations, while smaller scales are accounted for by a sub-grid scale (SGS) model.

Hydro3D has undergone rigorous validation, including assessments in channel flow<sup>31,32</sup> and scalar transport. The simulation of the coughing cloud aerosol concentration and absolute humidity is

expressed by two passive scalars, while its temperature is depicted by one active scalar.<sup>33,34</sup> A passive scalar is transported by the velocity field without influencing it, while an active scalar is not only transported by the velocity field but also undergoes changes and influences it. The discrete particle method (DPM), implemented and validated during the investigation of bubble plumes,<sup>35,36</sup> is incorporated in the simulations. The governing equations are as follows:

$$\frac{\partial(u_i)}{\partial x_i} = 0, \quad \frac{\partial(u_i)}{\partial t} + \frac{\partial(u_i u_j)}{\partial x_j} = -\frac{\partial p}{\partial x_i} + \nu \frac{\partial^2 u_i}{\partial x_i \partial x_j} - \frac{\partial \tau_{ij}}{\partial x_j} + f_i, \quad (1)$$

where  $t$  and  $\nu$  are, respectively, time and the kinematic viscosity,  $u_i$ ,  $u_j$  ( $i, j, k = 1, 2, 3$ ) is the filtered velocity vector in the three spatial directions ( $x, y, z$ ) stored at their respective cell faces while  $p$  is the filtered pressure which is stored in the center of the fluid cell. The geometries of the ventilations and mannequins are represented by an organized scatter of immersed boundary points (IBPs). The term  $f_i$  accounts for the external forces applied by the direct forcing immersed boundary method, ensuring a no-slip condition at every IBP.<sup>37</sup> The stress tensor  $\tau_{ij}$ , resulting from filtering, represents the unresolved small-scale or sub-grid scale (SGS) motion. The SGS stresses are approximated using the standard wall-adapting local eddy (WALE) viscosity model.<sup>38</sup> This model calculates the SGS viscosity implicitly to provide accurate dissipation. Unlike the Smagorinsky model, the WALE method does not require damping near solid walls, allowing for precise predictions of sub-grid scale viscosity near solid surfaces. This advantage is particularly evident when used in conjunction with the immersed boundary method,<sup>39</sup> where the grid does not follow solid surfaces. A fourth-order central differencing scheme discretizes the spatial first and second-order derivatives<sup>40</sup>—convection and diffusion terms—of the governing equation [Eq. (1)]. Time advancement is achieved through the fractional-step method.<sup>41</sup> A predictor–corrector method is employed to predict the intermediate non-divergence-free velocity field using a two-step Runge–Kutta scheme. These velocities are then projected onto a divergence-free vector field using the Poisson equation. Subsequently, the Poisson equation is solved using the multigrid method.

#### 2. Scalar phase

The transport of the concentration of the aerosol ( $d_p < 10 \mu\text{m}$ ), temperature, and humidity, e.g., due to a human puff resulting from breathing or coughing, is represented by solving the filtered scalar transport equation

$$\rho_{as} \frac{\partial \psi}{\partial t} + u_i \frac{\partial \psi}{\partial x_i} = (D + D_t) \frac{\partial^2 \psi}{\partial x_i^2} + S_i, \quad (2)$$

where  $\psi$  is the passive scalar (aerosol, temperature, and humidity),  $t$  is the time,  $u_i$  is the velocity, and  $x_i$  is the coordinate in the respective  $i, j, k$  directions,  $D$  represents the molecular diffusivity,  $D_t$  is the sub-grid scale turbulent diffusivity,  $S_i$  is the source term that accounts for gravity, and  $\rho_{as}$  defines the air–saliva mixture [ $\rho_{as} = \rho_a(1 - \Omega) + \Omega \rho_s$ ].<sup>42</sup>

#### 3. Discrete phase

The large droplets expelled ( $d_p \geq 50 \mu\text{m}$ ) during the physical process of a human cough are delineated by Lagrangian particles. These particles are assumed to be rigid, spherical, and to not deform or

coalesce. The motion of individual droplets is governed by Newton's second law

$$m_p \frac{\partial v_{p,i}}{\partial t} = F_{p,i}, \quad (3)$$

where  $m_p$  is the mass of the droplet,  $v_{p,i}$  is the droplet velocity in the three spatial directions  $i, j, k$ , and  $F_{p,i}$  defines the sum of the interfacial air forces acting on the droplet including buoyancy, fluid stress, added mass, drag, and lift. The buoyancy force is given by

$$F_G = (m_p - m_a)g, \quad (4)$$

where  $m_a$  accounts for the mass of air displaced by the droplet volume and subjected to the gravitational acceleration  $g$ . This buoyancy force is only applied in the vertical direction  $i=3$ . The fluid stress force describes the air resistance to the particle's acceleration

$$F_S = m_l \frac{\partial u_i}{\partial t}, \quad (5)$$

where  $u_i$  represents the air velocity at the droplet core location. The added mass defines the air resistance to the droplet displacement

$$F_A = -C_A m_l \frac{\partial}{\partial t} (u_{slip,i}), \quad (6)$$

where  $C_A$  is an empirical coefficient equal to 0.5 when considering a sphere and  $u_{slip,i}$  is the slip velocity, which is the difference between the droplet and air velocity ( $v_{p,i} - u_i$ ). The drag force exerted by the air onto the droplet in the direction of motion is defined as

$$F_D = \frac{1}{2} C_D \rho_a A |v_{p,i} - u_i| (v_{p,i} - u_i), \quad (7)$$

where  $A$  is the projected area of the droplet and  $\rho_a$  is the air density. The drag coefficient is calculated using a standard drag curve and is dependent on the droplet Reynolds number  $Re_p$  defined as

$$Re_p = d_p * \frac{\sqrt{u_{slip,1}^2 + u_{slip,2}^2 + u_{slip,3}^2}}{\nu}, \quad (8)$$

where  $\nu$  is the kinematic viscosity of air. The lift force exerted on the droplet is described as

$$F_L = -C_L m_p (v_{p,i} - u_i) \omega_i, \quad (9)$$

where  $\omega_i$  is the fluid vorticity and  $C_L = 0.53$  is the lift coefficient for a sphere.

#### 4. Evaporation phase

The evaporation model<sup>21,43</sup> couples the scalar phase with the discrete phase. This is based on the location of the droplet in or outside of the puff by using both the temperature and humidity scalar fields to calculate the evaporation rate of the discrete droplet and the change in diameter, which subsequently affects the integral forcing and dynamics of the droplet. The evaporation rate is defined as

$$\frac{\partial d_p}{\partial t} = \frac{-M_p D_v N_u}{d_p \rho_p R T_p} \Delta p, \quad (10)$$

where  $M_p$  is the molecular weight of the particle,  $D_v$  is the diffusion coefficient of water vapor, and  $N_u$  represents the Nusselt number

( $N_u = 1 + 0.276 Re_p^2 S_c^{1/3}$ ), which is the ratio between the convective mass transfer and the diffusion rate.  $R$  is the universal gas constant,  $T_p$  is the temperature at the surface of the droplet, and  $\Delta p$  is the droplet surface tension given by

$$\Delta p = p_t \times \ln \left( \frac{1 - p_{sat,T_p}/p_t}{1 - RH \times p_{sat,T_\infty}/p_t} \right), \quad (11)$$

where  $p_t$  is the atmospheric pressure,  $p_{sat}$  is the vapor pressure calculated using the buck formula, and  $RH$  is the relative humidity.

The physical experiment by Chaudhuri *et al.*<sup>44</sup> is reproduced numerically to validate the performance of the evaporation model, i.e., decoupled from the discrete particle method (DPM) framework. In their experiment, droplets of various sizes were introduced into an acoustic levitation chamber designed to keep the droplets motionless. It was necessary to remove motion in order to eliminate external forces, such as drag, and thereby allow for the quantification of the impact of temperature and relative humidity. Figure 1 shows that the numerical results agree fairly well with the experimental data when the droplets are considered fully motionless ( $Re=0$ ). The total evaporation time is over-predicted by the numerical model by a maximum of 40% for the small droplet ( $647 \mu\text{m}$ ) and only 11% for the large droplet ( $346 \mu\text{m}$ ). When the model accounts for the small vibration movement introduced by the acoustic levitation of the chamber wave, e.g., by considering  $Re=0.1$  as monitored in the experiment for a large droplet, the model's evaporation rate and time agree very well with the experimental data. However, vibrations appear to have less effect on the smaller droplet.

To gain a deeper understanding of how the temperature and humidity of the surrounding droplet affect its evaporation, we applied the evaporation model to a static droplet with a diameter of  $50 \mu\text{m}$ . The model was tested across a wide range of temperature and humidity conditions until the droplet completely evaporated (Fig. 2). The impact of humidity at a given temperature has a more significant effect

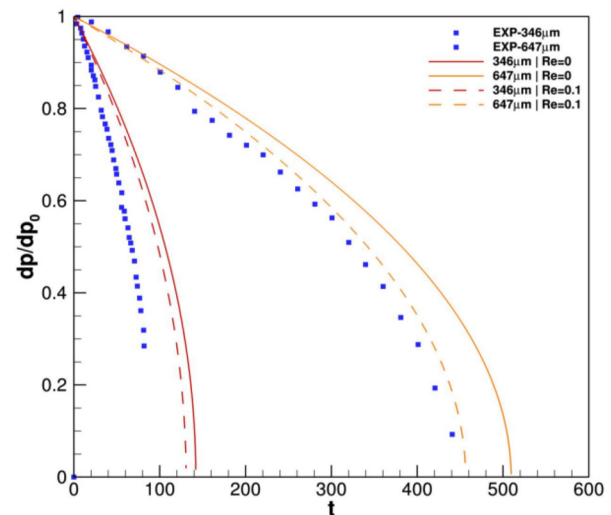


FIG. 1. Hypersonic levitation induced motionless evaporation of 346 and  $647 \mu\text{m}$  particles ( $T = 30^\circ$  and  $RH = 50\%$ ).

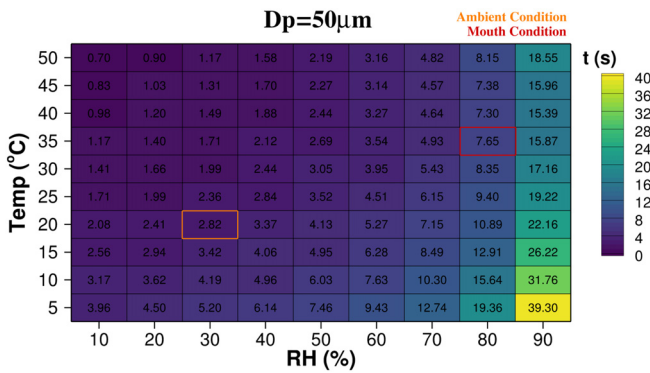


FIG. 2. Graph representing the time required for a static droplet of saliva to fully evaporate under different temperatures and relative humidities.

on the evaporation of a static droplet compared to the influence of temperature at a given humidity. In other words, droplet evaporation shows a stronger correlation with changes in humidity than with changes in temperature. The orange frame represents the time required for the 50 μm saliva droplet to evaporate in the Health Infrastructure Research Group (HIRG) unmixed environment under static conditions, while the red frame represents the time required for the droplet to evaporate in the infected mouth condition. It is evident that when the droplet is carried by the cough momentum from the infected mouth into the ambient room, its evaporation evolves in a non-linear manner. Figure 2 shows that the evaporation model is quite accurate as it predicts a static droplet of 50 μm to evaporate in 2.08 s when in an ambient room of 20 °C and a relative humidity of 10%; this finding is similar to the previous study.<sup>45</sup>

The evaporation model for pure water was validated. Moreover, in this study, a coughing event is investigated where saliva droplets are expelled. Saliva droplets are composed of water, protein, and salt. The mass fraction of salt and water directly affects the evaporation rate of the droplet. The mass fraction  $a_w$  was added to the evaporation model as introduced in the paper by Liu *et al.*<sup>46</sup>

The forward coupling between the absolute humidity passive scalar and the droplet surface tension term of the evaporation model is ensured by Eqs. (12)–(14)

$$P_v = AH * R_w * T_{inf}, \tag{12}$$

$$P_s = P_c * \exp \left[ \frac{T_c}{T_{inf}} (a_1 \tau + a_2 \tau^{1.5} + a_3 \tau^3 + a_4 \tau^{3.5} + a_5 \tau^4 + a_6 \tau^{7.5}) \right] \tag{13}$$

with  $T_c = 641.096$  K and  $P_c = 22064$  Pa, respectively, characterizing the critical temperature and pressure of water,  $\tau = 1 - (T/T_c)$ , and the following empirical constants  $a_1 = -7.860$ ,  $a_2 = 1.844$ ,  $a_3 = -11.787$ ,  $a_4 = 22.681$ ,  $a_5 = 1.801$ :

$$RH = \frac{P_v}{P_s} * 100. \tag{14}$$

These equations determine the relative humidity (RH) using the absolute humidity cloud scalar value, the vapor ( $P_v$ ), and saturation ( $P_s$ ) pressure.

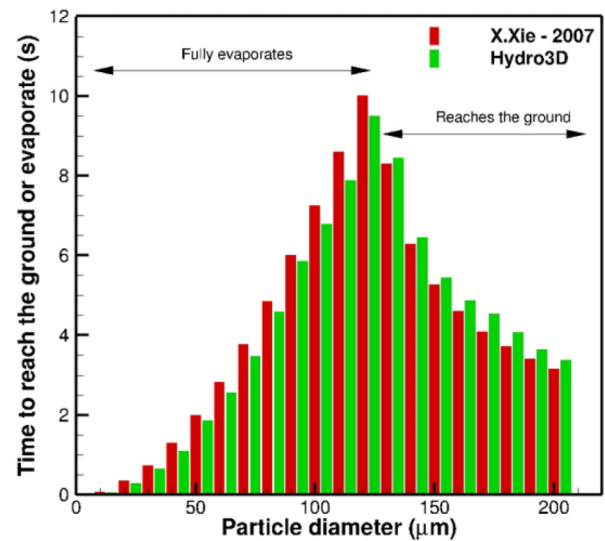


FIG. 3. Evaporation and falling time of numerous droplet sizes released at 2 m from the ground ( $T = 33^\circ$  and  $RH = 0\%$ ).

Subsequently, the validation of the coupling between the discrete phase and the evaporation phase was conducted through the simulation of a falling droplet from a height of 2 m to the ground (Fig. 3). This specific test case was executed by researcher Xie to assess the accuracy of his evaporate and discrete phase models, and our results demonstrate a great level of agreement with his findings.

### B. Numerical simulation of a droplet dynamics experiment

The numerical reproduction of the experiment of the Health Infrastructure Research Group (HIRG) was undertaken in order to assess the evaporation model when coupled with the computational fluid dynamics (CFD) and DPM frameworks. In this experiment, droplets with different diameters ranging from 10 to 200 μm were released at a height of 2 m from the ground. In Hydro3D, only the gravity and the drag force significantly impact the dynamics of a falling droplet. In the experiment, larger droplets ( $d_p > 120$  μm) fell to the ground without fully evaporating, while smaller droplets ( $d_p < 120$  μm) fully evaporated before reaching the ground. It is important to note that the droplets used in this experiment were made of pure water and did not fully represent the bio-physical properties of saliva droplets; proteins and salt in saliva prevent complete evaporation and constitute the nuclei of the solid form of the droplets. The final diameter of the solid form was found experimentally to range between 18% and 24% of the initial droplet diameter ( $d_{p0}$ ) at  $t_0$ .

The simulations are performed representing a domain that is identical in size to the HIRG chamber, which is depicted in Fig. 4. For the unmixed environment, all chamber fans are deactivated, while for the mixed environment, the mixing and outlet fans are turned on. The boundary condition for the mixing fan in the CFD is set as a downward vertical velocity of 3.5 m/s, while the outlet fan is set as a Neumann boundary condition ensuring mass conservation in this closed room system. The room had a square floor plate of dimensions



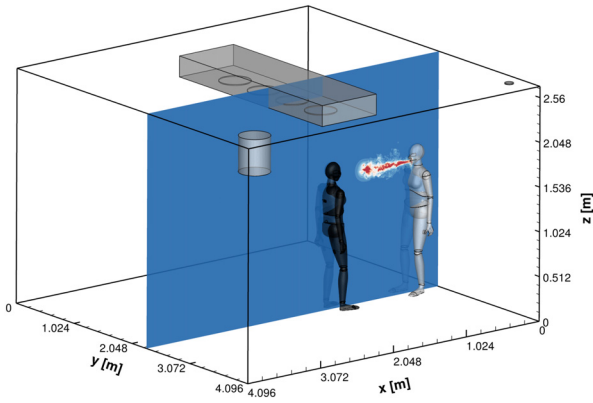


FIG. 4. Computational domain representing the HIRG chamber at UCL facilities.

$4.1 \times 4.1 \text{ m}^2$  and was 2.7 m high so that the total air volume was around  $45 \text{ m}^3$ . In the experiment, the room temperature ( $22.4 \text{ }^\circ\text{C}$ ) and humidity ( $32\%/6.359 \text{ g/m}^3$ ) were measured using an anemometer and details are given in the following table. Given the time frame (seconds) of the simulation, the temperature and the humidity in the room are considered constant. In the simulation, the coughing from the individual's mouth is represented by a rectangle of  $20 \times 50 \text{ mm}^2$  with a coughing velocity peaking at  $8.4 \text{ m/s}$ , ensuring the same volumetric flow as in the study by Gupta *et al.*<sup>47</sup> Subsequently, both the infected and healthy individuals have a standard breathing cycle.<sup>8</sup> The temperature ( $34 \text{ }^\circ\text{C}$ ) and humidity ( $85\%/31.93 \text{ g/m}^3$ ) during coughing and breathing are the same. Droplets are only expelled during the coughing event from the infected individual, and the distribution of the droplet size ranges between  $10$  and  $200 \text{ }\mu\text{m}$ , which is based on the experimental investigation by Lindsley *et al.*<sup>48</sup> The correlation between the number of particles and their time of release during a coughing event is not well-known in the current scientific literature. This is a highly chaotic phenomenon, and therefore, the whole pool of particle sizes to be expelled is randomized, and a correlation between the number of particles released and the flux of the coughing event is established (Fig. 5).

Simulation properties	Symbols	Values
<b>Room</b>		
Temperature	T	$22.4 \text{ }^\circ\text{C}$
Relative humidity	RH	32%
Absolute humidity	AH	$6.359 \text{ g/m}^3$
Inlet fan velocity	$U_{in}$	$6.8 \text{ m/s}$
Outlet fan velocity	$U_{out}$	$0.75 \text{ m/s}$
<b>Cloud gaseous phase</b>		
Temperature	T	$34 \text{ }^\circ\text{C}$
Humidity	RH	85%
Absolute humidity	AH	$31.93 \text{ g/m}^3$
Density	$\rho_f$	$1.204 \text{ kg/m}^3$
Peak velocity	$U_{peak}$	$8.4 \text{ m/s}$
<b>Particle discrete phase</b>		
Density	$\rho_p$	$993 \text{ kg/m}^3$
Droplet velocity	$\nu_p$	$0.2\text{--}8.4 \text{ m/s}$

The relative size difference between the mannequin mouth volume ( $0.020 \times 0.020 \times 0.050 \text{ m}^3$ ) and the HIRG room ( $2.7 \times 4.1 \times 4.1 \text{ m}^3$ ) presents clear challenges in simulating an accurate, high-fidelity coughing puff in such a large space while adhering to computational cost limitations. Mesh sensitivity analysis was performed in the smaller open domain ( $2.048 \times 1.028 \times 1.028 \text{ m}^3$ ). Three uniform meshes were tested: coarse (32 mm), medium (16 mm), and refined (8 mm). The computational spanned over 2 s, with the coughing occurring in the first 0.5 s and propagating during the next 1.5 s. The mean streamwise velocity was averaged throughout the computational time. The sensitivity analysis ensured the convergence of streamwise momentum. The mean streamwise velocity, normalized with the maximum streamwise velocity values, is displayed in Fig. 6. Frames 1–3 represent the coarse, medium, and refined grids, respectively. Mesh refinement not only affects cloud diffusion/dispersion but also influences the velocity magnitude within the cloud puff. The coarse mesh displays a velocity contour covering a wider volume in the domain, with a reduced velocity magnitude near the mouth of the mannequin compared to the medium and fine meshes. This observation is supported by Fig. 6(d), which quantitatively

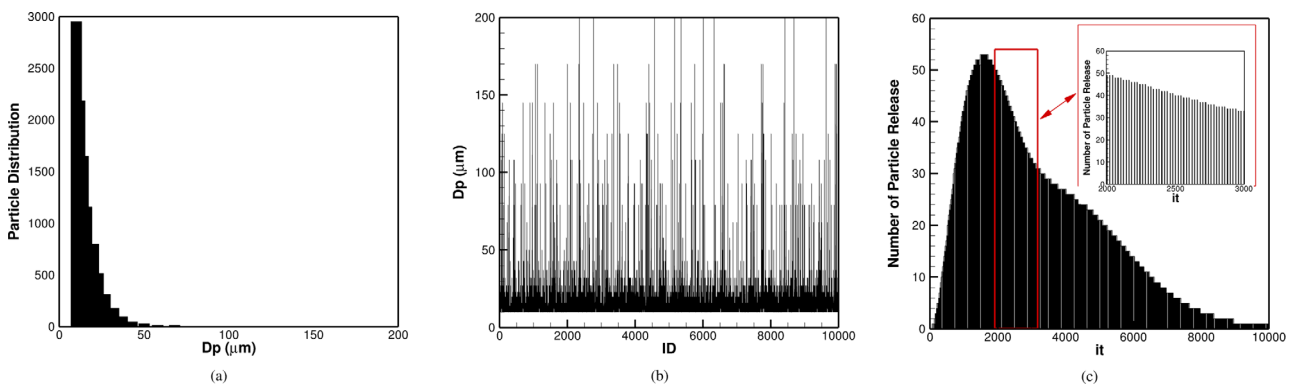
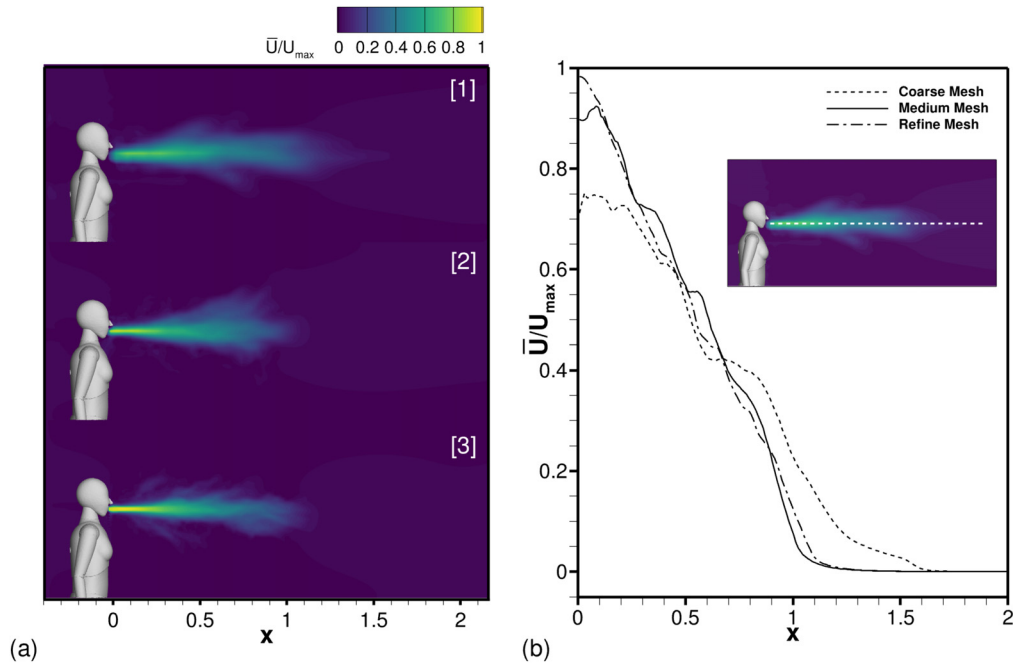


FIG. 5. Graphs representing the methodology used for the delivery of the discrete phase droplets: (a) particle distribution (Lindsley *et al.*<sup>48</sup>), (b) mixing of all the particle bins and randomized allocation of the droplet ID, (c) number of droplets released correlates to the mass expelled (Gudta *et al.*<sup>47</sup>).



**FIG. 6.** Mean streamwise velocity contour during a coughing event (a) coarse, (b) medium, (c) refine mesh resolution, and (d) evolution of the mean streamwise velocity over the 2 m centerline of the cough.

captures the evolution of the mean streamwise velocity along the centerline of the cough, spanning from the mouth of the mannequin to the end of the domain. Centerline values near the mouth exhibit a lower streamwise velocity ( $-20\%$ ) compared to the medium and fine meshes. The extremity of the cloud on the centerline along the  $x$ -axis is located at 1.6 m for the coarse mesh, while it is around 1.2 m for both the medium and fine meshes. The medium and fine meshes exhibit similar cloud behavior, with the medium mesh showing a slight momentum difference near the mouth ( $-5\%$ ) while being marginally more diffused. The medium and refined meshes provided similar results, while the computational cost of the medium mesh remains significantly cheaper. For this reason, the medium mesh was chosen for the HIRG simulations to evaluate the impact of an unmixed and mixed environment on the cloud and droplet dynamics.

The HIRG chamber was simulated for 10 s of computational time with a resolution of  $12 \times 10^6$  cells using the uniform medium mesh. The computational domain was divided into 240 subdomains and runs in parallel using a hybrid method using MPI tasks and OpenMP threads. The simulations are performed on 80 processors of the Intel (R) Xeon(R) Gold 6138 CPU @ 2.00 GHz, with a total duration of 9600 CPU hours for the largest simulation.

### III. RESULTS AND DISCUSSION

The particle Reynolds number, temperature, and humidity, which directly affect the evaporation of large droplets, are recorded at each time step throughout the simulation. A dataset of 50 000–100 000 time steps is collected for each particle. The time-averaged values of the three aforementioned properties are calculated for each DPM particle representing the large droplets. Each of these particles belongs to a group/bin defined by their initial diameter (Fig. 5). A boxplot statistical

analysis was performed to further understand the behavior of these different droplet size groups during a coughing event (Fig. 7).

The probability density function of the Reynolds number for various initial particles under unmixed steady conditions is displayed in Fig. 8. The average Reynolds number of the particles ranges from 0.02 to 7.95. The Box-Whisker plot is influenced by the coughing flux at the time of particle release, which affects the skewness of some particle bins, such as those for 79, 170, and 200  $\mu\text{m}$ . For particles larger than 100  $\mu\text{m}$ , the plot reveals a few low outliers, which could be attributed to the fact that these large particles quickly fall out from the puff (initial cloud).

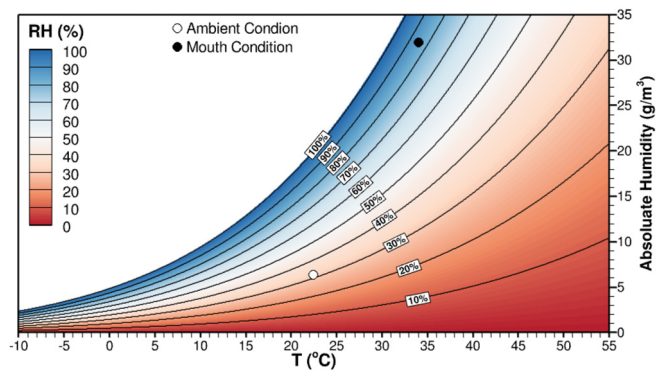


**FIG. 7.** Psychrometric graph<sup>49</sup> which relates the absolute humidity (passive scalar) and the temperature (active scalar) to the relative humidity used in the evaporation model. The droplet's evaporated volume is coupled to the absolute humidity passive scalar. The orange dot represents the ambient air room condition, while the red dot describes the air expelled during a coughing cycle.

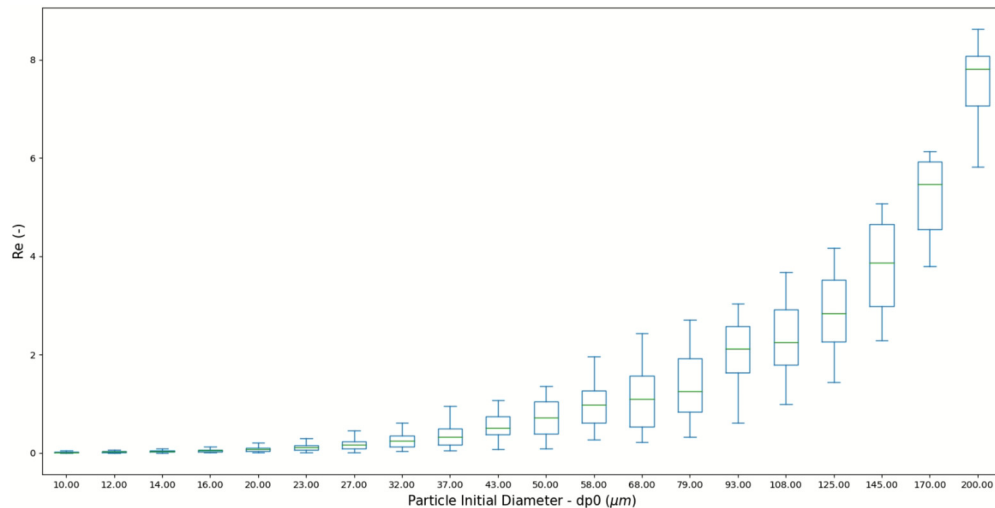


**FIG. 8.** This Box-Whisker graph represents the probability density function of each particle bin average Reynolds number. The x-axis represents each initial particle diameter sizing, while the y-axis defines the average Reynolds number that each bin particle is subjected to during the simulation.

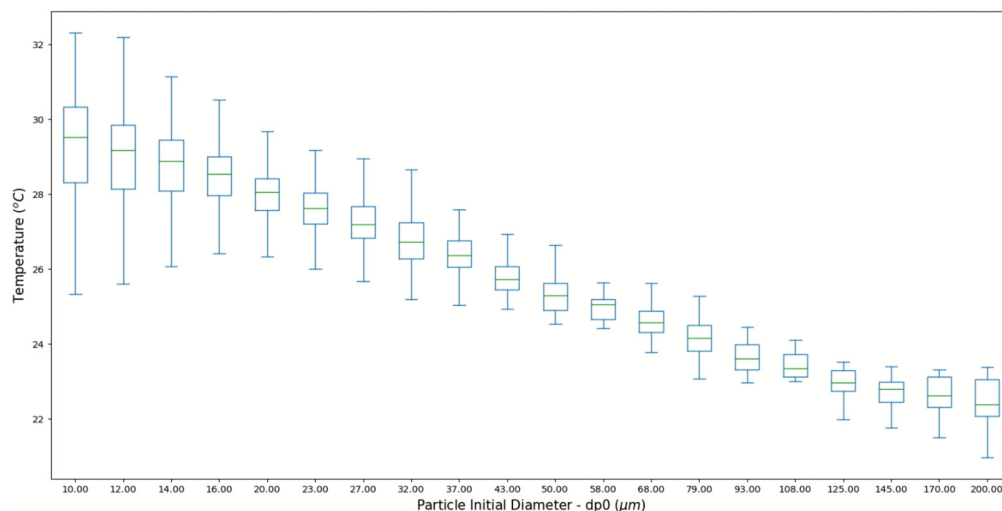


**FIG. 9.** Box-Whisker graph that captures the mean temperature distribution acting on each particle sizing.

The influence of the particles' position within the cloud, leading to significant changes in the droplets' average temperature and absolute humidity during their evaporation, is illustrated in Figs. 9 and 10. The smaller the droplet, the higher the temperature and relative humidity, as they are closer to the infected human's mouth. Larger droplets require more time to evaporate and they can travel further away from the mouth due to their momentum. This highlights the importance of the forward coupling from the active temperature scalar and passive humidity scalar to the single particle evaporation model. The average temperature acting on the droplets ranges from 22.6 °C to 29.8 °C, while the average absolute humidity ranges from 9.5 to 24.6 g/m<sup>3</sup>. Smaller particles have a higher outlier difference compared to particles above 100 μm. This particularly demonstrates a greater

influence of the cloud velocity field on small particles, moving a portion of them to its extremity, also called the interface between the cloud and the ambient room conditions.

Figure 11 shows locations where large droplets land on a healthy individual in both unmixed and mixed environments. Most particles had fully evaporated upon reaching the individual. A total of 2851 droplets ended up on the receiving human; most of them landed on the upper part of the chest and on the face. The number of large droplets inhaled by the receiving human represented 28.5% of the number of droplets emitted by the infected human. In the mixed environment, most of the particles landed between the lower chest and the hips, greatly reducing the number of droplets traveling onto the face and, thus, into the respiratory parts. In this specific room setting and



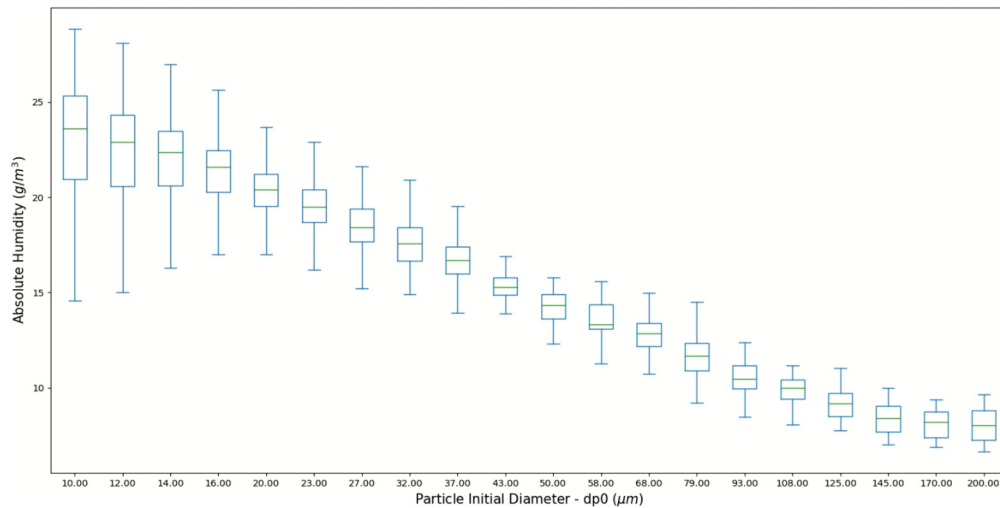


FIG. 10. Box-Whisker graph that captures the mean absolute humidity distribution acting on each particle sizing.

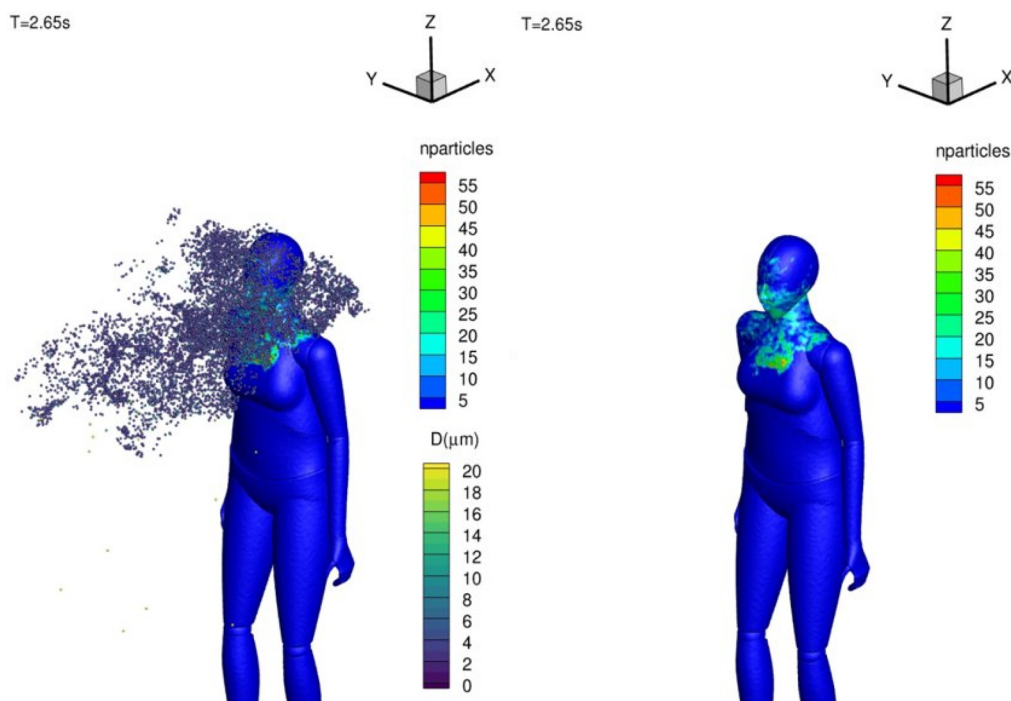


FIG. 11. Infected droplet exposition from the healthy individual looking 1 m away from the infected host.

mixing boundary condition, the mixed environment resulted in a faster dispersion of the aerosols, significantly impacting the droplet dynamics and reducing the risk of infection for the healthy individual.

The 2D contours of velocity magnitude, aerosol concentration (scalar), temperature, and absolute humidity in both fully mixed and unmixed environments are shown in Figs. 12 and 14. A clear distinction can be observed in the velocity magnitude when comparing the

unmixed and mixed environments. In the unmixed environment, the coughing puff disperses toward the healthy individual and is clearly visible, whereas in the mixed environment, it is barely visible due to the velocity disturbance between the two humans. The aerosol cloud in Fig. 13 displays a distinct direction of propagation in the mixed environment, indicating a clear downward-pull which is imposed by the mixing fan at the ceiling. The same phenomenon is displayed in

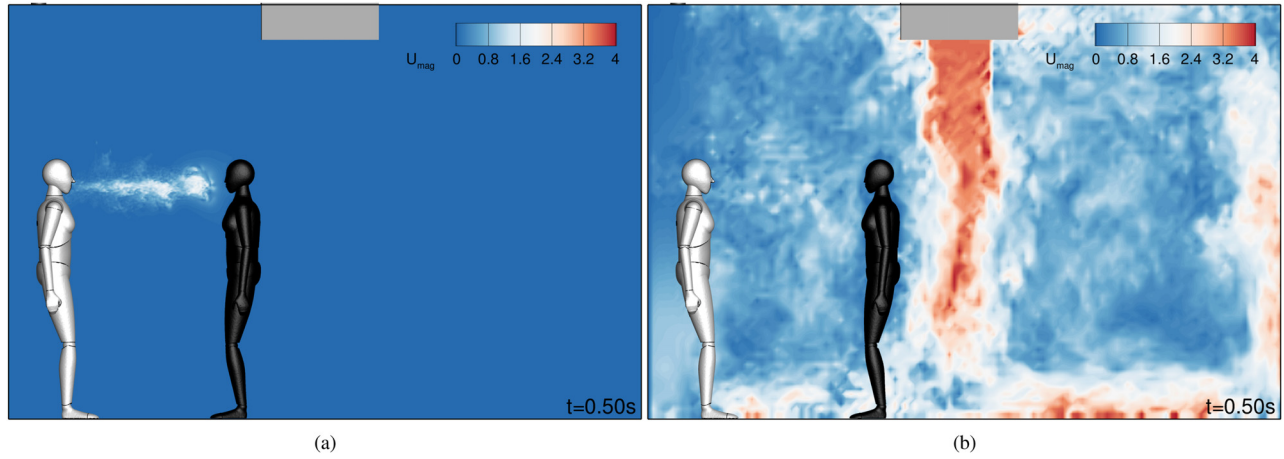


FIG. 12. Velocity magnitude contour in non-mixed (a) and mixed (b) environments.

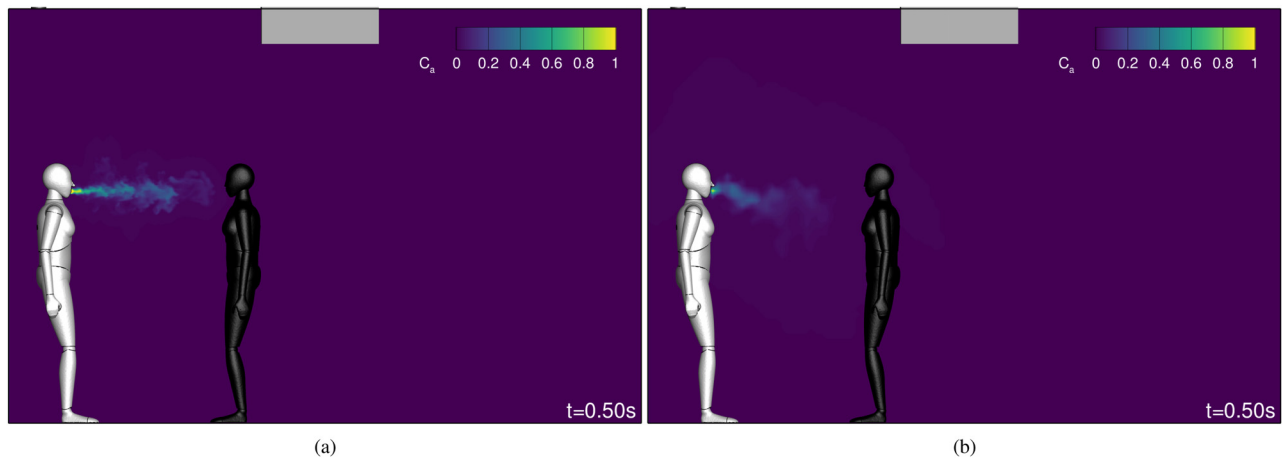


FIG. 13. Aerosol contour in non-mixed (a) and mixed (b) environments.

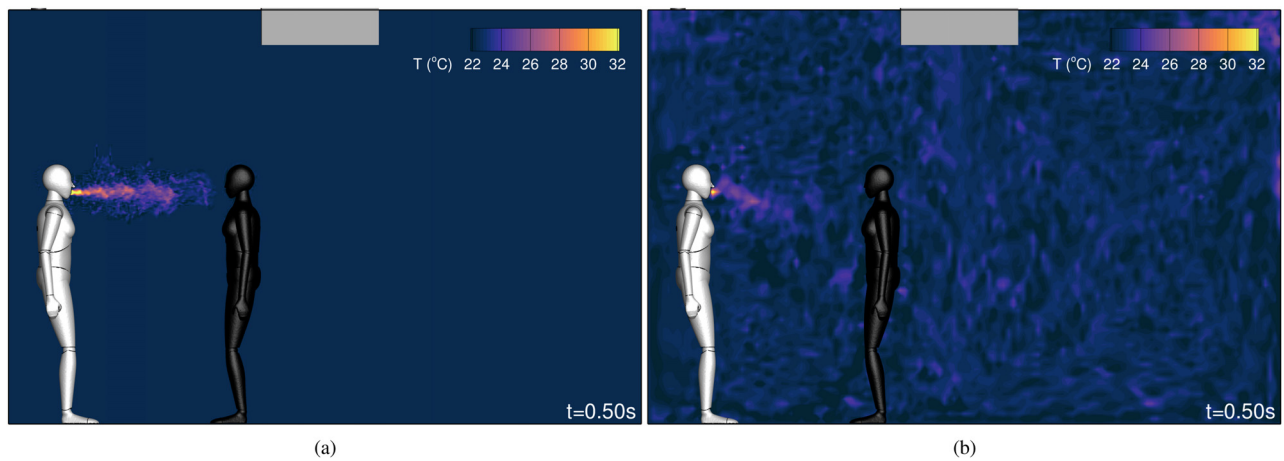


FIG. 14. Temperature contour in non-mixed (a) and mixed (b) environments.

13 March 2024 21:05:08

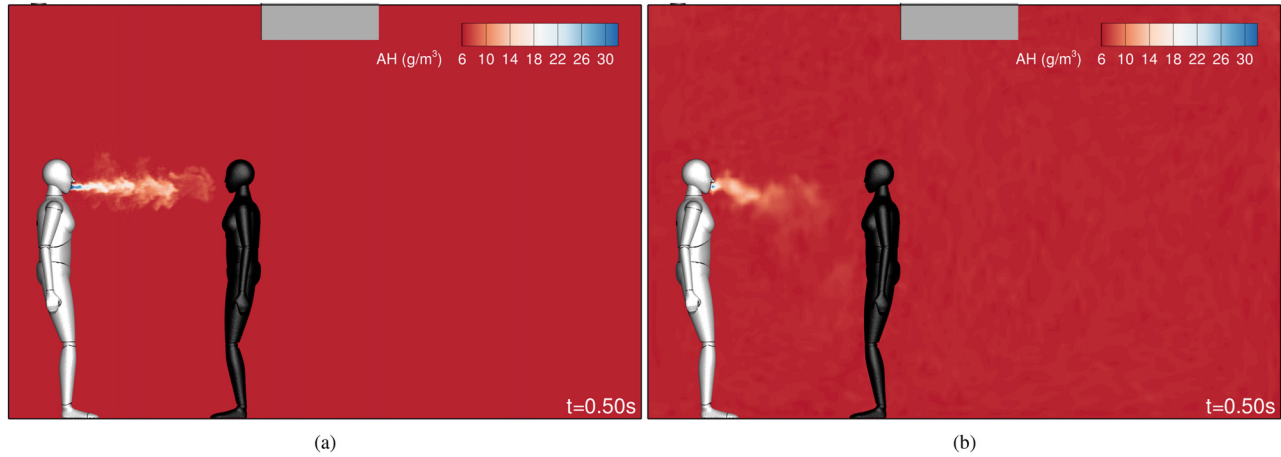


FIG. 15. Absolute humidity contour in non-mixed (a) and mixed (b) environments.

the absolute humidity contour plot, where less momentum is conserved from the coughing cloud when facing a highly disturbed environment, impeding its efficiency in reaching and infecting a healthy individual (Fig. 15).

The state of evaporation of large droplets is depicted in Fig. 16, ranging from fully evaporated (Evap = 0) to not evaporated (Evap = 1) in both unmixed and mixed environments. In both environments, 0.5 s after the beginning of the coughing event, the majority of droplets are already fully evaporated and are being carried in their nuclei state. The droplets that are still evaporating are above 50 μm in both environments. There is a clear impact of fully mixed flow on the dynamics of large droplets. The flow produced by the mixing fan exerts a downward pulling force on the large droplet cloud, creating an angle of incidence that causes the droplets to stick to the chest of the healthy host in the unmixed environment, whereas they reach the face of the healthy host in the mixed environment, as shown in Fig. 11.

The analysis of liquid penetration distance enables a further quantification of the evaporation model in the two distinct unmixed and mixed environments. The liquid penetration distance evaluates

the distance that the droplets reach when 5% of their mass has evaporated or 95% of their mass remains. In both mixed and unmixed environments, similar results are observed for droplets with initial diameters of 20 μm. The liquid penetration distance averages at 10 cm away from the mouth of the coughing individual. For particles ranging from 20 to 100 μm, the liquid penetration distance is reduced by 30% in the mixed environment. Larger droplets above 100 μm are less affected due to the initial conditions set by the initial cough, and the distance is reduced by 5% in the mixed environment. Regardless of the environment, the results align with the liquid penetration findings in the study by Dbouk and Drikakis<sup>45</sup> when there is no wind. This is likely attributed to the direction of ventilation, which is perpendicular to the coughing direction, as opposed to being parallel as in the aforementioned paper.

The impact of the evaporation volume on the active temperature and passive absolute relative humidity is revealed in Fig. 17. However, its influence on the temperature and absolute humidity of the cloud is negligible. The average temperature change imposed on the computational cell where an individual particle is located reaches a maximum

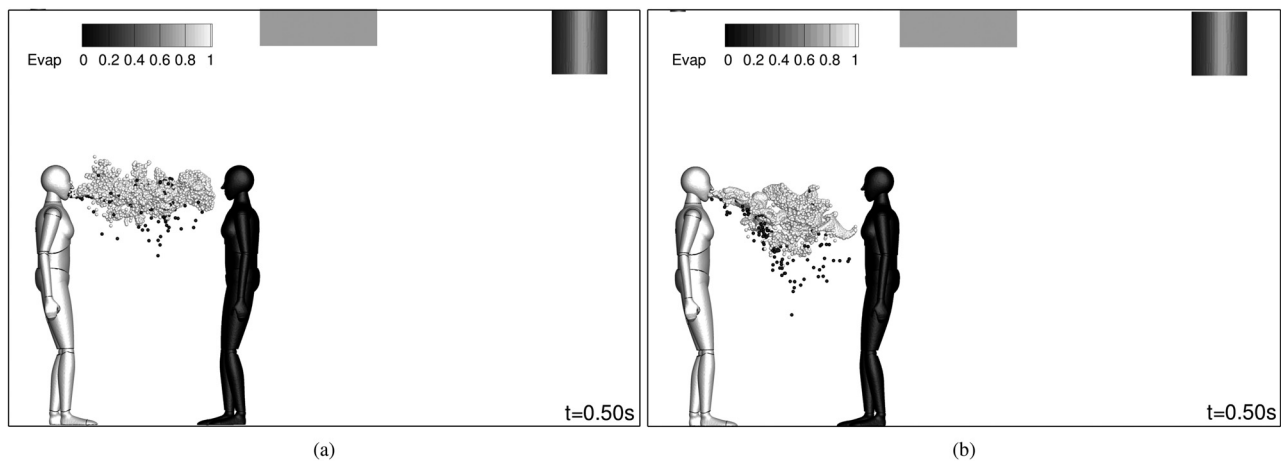


FIG. 16. Evaporation state of the LPT particles. When Evap = 0, the particle fully evaporated, and when Evap = 1, the particle is still evaporating.

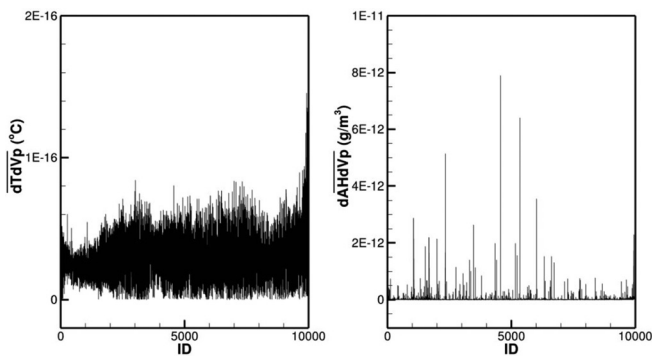


FIG. 17. Change in (a) temperature and (b) humidity within the expelled cloud ensuing from the evaporation of each individual droplet.

of  $1E - 16^{\circ}\text{C}$ , while for the absolute humidity, it is a maximum of  $8E - 12\text{ g/m}^3$ . This result indicates that although the model is coupled both forward and backward, the backward coupling is not necessary for this instance due to the small size of the droplets. Nevertheless, it remains an interesting framework for other applications that use much larger droplets.

#### IV. SUMMARY AND CONCLUSIONS

This study has made significant advancements in understanding the dispersion and behavior of particles expelled during a coughing event in two different environmental conditions. High-fidelity simulations of coughing events were conducted in both mixed and unmixed environments, providing valuable insight into the dynamics of particle dispersion.

The coupling of temperature and humidity scalars with the evaporation model revealed a substantial impact on particle behavior. Smaller particles exhibited faster dispersion within the cough cloud and experienced greater variations in temperature and humidity. The Reynolds numbers of the particles ranged from 0.2 to 8.

The mixed environment significantly influenced the cough cloud's behavior, leading to accelerated droplet evaporation and a reduction in the number of particles inhaled by the mannequin. This highlights the importance of environmental factors in particle dispersion.

Proper ventilation can lead to a substantial reduction in the potential transmission of pathogens, significantly in mitigating the spread of infectious diseases.

#### ACKNOWLEDGMENTS

This research was funded by the Airborne Infection Reduction through Building Operation and Design for SARS-CoV-2-AIRBODS (EPSRC Grant No. EP/W002779/1) project. We are grateful for the cooperation and help received from laboratory staff at University College London.

#### AUTHOR DECLARATIONS

##### Conflict of Interest

The authors have no conflicts to disclose.

#### Author Contributions

**Arthur Hajaali:** Conceptualization (equal); Formal analysis (lead); Investigation (lead); Methodology (equal); Writing – review & editing (equal). **Thorsten Stoesser:** Conceptualization (equal); Methodology (equal); Supervision (equal); Writing – review & editing (equal). **Shaun Fitzgerald:** Conceptualization (equal); Methodology (equal); Supervision (equal); Writing – review & editing (equal).

#### DATA AVAILABILITY

The data that support the findings of this study are available from the corresponding author upon reasonable request.

#### REFERENCES

- <sup>1</sup>L. Bourouiba, E. Dehandschoewercker, and J. Bush, "Violent expiratory events: On coughing and sneezing," *J. Fluid Mech.* **745**, 537–563 (2014).
- <sup>2</sup>L. Bourouiba, "Turbulent gas clouds and respiratory pathogen emissions: Potential implications for reducing transmission of COVID-19," *JAMA* **323**(18), 1837–1838 (2020).
- <sup>3</sup>X. Xie, Y. Li, H. Sun, and L. Liu, "Exhaled droplets due to talking and coughing," *J. R. Soc. Interface* **6**, S703–S714 (2009).
- <sup>4</sup>S.-B. Kwon, J. Park, J. Jang, Y. Cho, D.-S. Park, C. Kim, G.-N. Bae, and A. Jang, "Study on the initial velocity distribution of exhaled air from coughing and speaking," *Chemosphere* **87**, 1260–1264 (2012).
- <sup>5</sup>R. R. Netz, "Mechanisms of airborne infection via evaporating and sedimenting droplets produced by speaking," *J. Phys. Chem. B* **124**, 7093–7101 (2020).
- <sup>6</sup>K. M. A. Ho, H. Davies, R. Epstein, P. Bassett, i Hogan, Y. Kabir, J. Rubin, G. Y. Shin, J. P. Reid, R. Torii, M. K. Tiwari, R. Balachandran, and L. B. Lovat, "Spatiotemporal droplet dispersion measurements demonstrate face masks reduce risks from singing," *Sci. Rep.* **11**, 24183 (2021).
- <sup>7</sup>S. Asadi, A. S. Wexler, C. D. Cappa, S. Barreda, N. M. Bouvier, and W. D. Ristenpart, "Aerosol emission and superemission during human speech increase with voice loudness," *Sci. Rep.* **9**, 2348 (2019).
- <sup>8</sup>P. Bahl, C. M. de Silva, C. R. MacIntyre, A. A. Chughtai, and C. Doolan, "An experimental framework to capture droplets expelled during various respiratory exhalations," in *Proceedings of the 22nd Australasian Fluid Mechanics Conference (AFMC2020)* (University of Queensland, Brisbane, Australia, 2020).
- <sup>9</sup>F. K. A. Gregson, N. A. Watson, C. M. Orton, A. E. Haddrell, L. P. McCarthy, T. J. R. Finnie, N. Gent, G. C. Donaldson, P. L. Shah, J. D. Calder, B. R. Bzdek, D. Costello, and J. P. Reid, "Comparing aerosol concentrations and particle size distributions generated by singing, speaking and breathing," *Aerosol Sci. Technol.* **55**, 681–691 (2021).
- <sup>10</sup>M. Abuhegazy, K. Talaat, O. Anderoglu, and S. V. Poroseva, "Numerical investigation of aerosol transport in a classroom with relevance to COVID-19," *Phys. Fluids* **32**, 103311 (2020).
- <sup>11</sup>A. Agrawal and R. Bhardwaj, "Reducing chances of COVID-19 infection by a cough cloud in a closed space," *Phys. Fluids* **32**, 101704 (2020).
- <sup>12</sup>R. K. Bhagat, M. S. Davies Wykes, S. B. Dalziel, and P. F. Linden, "Effects of ventilation on the indoor spread of COVID-19," *J. Fluid Mech.* **903**, F1 (2020).
- <sup>13</sup>Y. Zhou and S. Ji, "Experimental and numerical study on the transport of droplet aerosols generated by occupants in a fever clinic," *Build. Environ.* **187**, 107402 (2021).
- <sup>14</sup>J. Quiñones, A. Doosttalab, S. Sokolowski, R. M. Voyles, V. Castaño, L. T. Zhang, and L. Castillo, "Prediction of respiratory droplets evolution for safer academic facilities planning amid COVID-19 and future pandemics: A numerical approach," *J. Build. Eng.* **54**, 104593 (2022).
- <sup>15</sup>H. Li, F. Y. Leong, G. Xu, Z. Ge, C. W. Kang, and K. H. Lim, "Dispersion of evaporating cough droplets in tropical outdoor environment," *Phys. Fluids* **32**, 113301 (2020).
- <sup>16</sup>K. L. Chong, C. S. Ng, N. Hori, R. Yang, R. Verzicco, and D. Lohse, "Extended lifetime of respiratory droplets in a turbulent vapor puff and its implications on airborne disease transmission," *Phys. Rev. Lett.* **126**, 034502 (2021).
- <sup>17</sup>C. S. Ng, K. L. Chong, R. Yang, M. Li, R. Verzicco, and D. Lohse, "Growth of respiratory droplets in cold and humid air," *Phys. Rev. Fluids* **6**, 054303 (2021).



- <sup>18</sup>J. K. Gupta, C.-H. Lin, and Q. Chen, “Characterizing exhaled airflow from breathing and talking,” *Indoor Air* **20**, 31–39 (2010).
- <sup>19</sup>K. Mahjoub Mohammed Merghani, B. Sagot, E. Gehin, G. Da, and C. Motzkus, “A review on the applied techniques of exhaled airflow and droplets characterization,” *Indoor Air* **31**, 7–25 (2021).
- <sup>20</sup>S. Sazhin, A. Elwardany, P. Krutitskii, G. Castanet, F. Lemoine, E. Sazhina, and M. Heikal, “A simplified model for bi-component droplet heating and evaporation,” *Int. J. Heat Mass Transfer* **53**, 4495–4505 (2010).
- <sup>21</sup>H. J. Holterman, “Kinetics and evaporation of water drops in air,” IMAG Report 2003-12 (2003), p. 67.
- <sup>22</sup>J. Redrow, S. Mao, I. Celik, J. A. Posada, and Z-g Feng, “Modeling the evaporation and dispersion of airborne sputum droplets expelled from a human cough,” *Build. Environ.* **46**, 2042–2051 (2011).
- <sup>23</sup>M.-R. Pendar and J. C. Páscoa, “Numerical modeling of the distribution of virus carrying saliva droplets during sneeze and cough,” *Phys. Fluids* **32**, 083305 (2020).
- <sup>24</sup>C. Lieber, S. Melekidis, R. Koch, and H.-J. Bauer, “Insights into the evaporation characteristics of saliva droplets and aerosols: Levitation experiments and numerical modeling,” *J. Aerosol Sci.* **154**, 105760 (2021).
- <sup>25</sup>B. Zhao, Z. Zhang, and X. Li, “Numerical study of the transport of droplets or particles generated by respiratory system indoors,” *Build. Environ.* **40**, 1032–1039 (2005).
- <sup>26</sup>F. Akagi, I. Haraga, S.—I. Inage, and K. Akiyoshi, “Effect of sneezing on the flow around a face shield,” *Phys. Fluids* **32**, 127105 (2020).
- <sup>27</sup>P. Katre, S. Banerjee, S. Balusamy, and K. C. Sahu, “Fluid dynamics of respiratory droplets in the context of COVID-19: Airborne and surfaceborne transmissions,” *Phys. Fluids* **33**, 081302 (2021).
- <sup>28</sup>T. Dbouk and D. Drikakis, “Weather impact on airborne coronavirus survival,” *Phys. Fluids* **32**, 093312 (2020).
- <sup>29</sup>M. Auvinen, J. Kuula, and T. Gro, “High-resolution large-eddy simulation of indoor turbulence and its effect on airborne transmission of respiratory pathogens-Model validation and infection probability analysis,” *Phys. Fluids* **34**, 015124 (2022).
- <sup>30</sup>T. Dbouk and D. Drikakis, “On airborne virus transmission in elevators and confined spaces,” *Phys. Fluids* **33**, 011905 (2021).
- <sup>31</sup>S. Bomminayuni and T. Stoesser, “Turbulence statistics in an open-channel flow over a rough bed,” *J. Hydraul. Eng.* **137**, 1347–1358 (2011).
- <sup>32</sup>T. Stoesser, R. McSherry, and B. Fraga, “Secondary currents and turbulence over a non-uniformly roughened open-channel bed,” *Water* **7**, 4896–4913 (2015).
- <sup>33</sup>S. Bomminayuni, S. Thorsten, and R. Nils, “Dispersion of a passive scalar in turbulent open channel flow,” in *River Flow* (CRC Press, 2014).
- <sup>34</sup>P. Ouro, B. Fraga, N. Viti, A. Angeloudis, T. Stoesser, and C. Gualtieri, “Instantaneous transport of a passive scalar in a turbulent separated flow,” *Environ. Fluid Mech.* **18**, 487–513 (2018).
- <sup>35</sup>B. Fraga and T. Stoesser, “Influence of bubble size, diffuser width, and flow rate on the integral behavior of bubble plumes: Integral behavior of bubble plumes,” *J. Geophys. Res.* **121**, 3887–3904, <https://doi.org/10.1002/2015JC011381> (2016).
- <sup>36</sup>B. Fraga, T. Stoesser, C. C. Lai, and S. A. Socolofsky, “A LES-based Eulerian-Lagrangian approach to predict the dynamics of bubble plumes,” *Ocean Modell.* **97**, 27–36 (2016).
- <sup>37</sup>M. Uhlmann, “An immersed boundary method with direct forcing for the simulation of particulate flows,” *J. Comput. Phys.* **209**, 448–476 (2005); [arXiv:1809.08170](https://arxiv.org/abs/1809.08170).
- <sup>38</sup>F. Nicoud and F. Ducros, “Subgrid-scale stress modelling based on the square of the velocity gradient tensor,” *Flow, Turbul. Combust.* **62**, 183–200 (1999).
- <sup>39</sup>M. C. Kara, T. Stoesser, and R. McSherry, “Calculation of fluid-structure interaction: Methods, refinements, applications,” in *Proceedings of the Institution of Civil Engineers-Engineering and Computational Mechanics* (Thomas Telford Ltd, 2015), Vol. 168, pp. 59–78.
- <sup>40</sup>M. Cevheri, R. McSherry, and T. Stoesser, “A local mesh refinement approach for large-eddy simulations of turbulent flows: Local mesh refinement for LES,” *Numer. Methods Fluids* **82**, 261–285 (2016).
- <sup>41</sup>A. J. Chorin, “Numerical solution of the Navier-Stokes equations,” *Math. Comp.* **22**, 745–762 (1968).
- <sup>42</sup>A. Khosronejad, C. Santoni, K. Flora, Z. Zhang, S. Kang, S. Payabvash, and F. Sotiropoulos, “Fluid dynamics simulations show that facial masks can suppress the spread of COVID-19 in indoor environments,” *AIP Adv.* **10**, 125109 (2020).
- <sup>43</sup>H. Wang, Z. Li, X. Zhang, L. Zhu, Y. Liu, and S. Wang, “The motion of respiratory droplets produced by coughing,” *Phys. Fluids* **32**, 125102 (2020).
- <sup>44</sup>S. Chaudhuri, S. Basu, P. Kabi, V. R. Unni, and A. Saha, “Modeling the role of respiratory droplets in Covid-19 type pandemics,” *Phys. Fluids* **32**, 063309 (2020).
- <sup>45</sup>T. Dbouk and D. Drikakis, “On coughing and airborne droplet transmission to humans,” *Phys. Fluids* **32**, 053310 (2020).
- <sup>46</sup>L. Liu, J. Wei, Y. Li, and A. Ooi, “Evaporation and dispersion of respiratory droplets from coughing,” *Indoor Air* **27**, 179–190 (2017).
- <sup>47</sup>J. K. Gupta, C.-H. Lin, and Q. Chen, “Flow dynamics and characterization of a cough: Flow dynamics and characterization of a cough,” *Indoor Air* **19**, 517–525 (2009).
- <sup>48</sup>W. G. Lindsley, J. D. Noti, F. M. Blachere, J. V. Szalajda, and D. H. Beezhold, “Efficacy of face shields against cough aerosol droplets from a cough simulator,” *J. Occup. Environ. Hygiene* **11**, 509–518 (2014).
- <sup>49</sup>A. B. Chambers, “A psychometric chart for physiological research,” *J. Appl. Physiol.* **29**, 406–412 (1970).